A Simulation Study on Characterizing Transfer Functions of Railway Tracks Using Train-Borne Laser Doppler Vibrometer

Zeng, Yuanchen; Núñez, Alfredo; Li, Zili

DOI
10.1007/978-3-031-39109-5_19

Publication date
2023

Document Version
Final published version

Published in
Experimental Vibration Analysis for Civil Engineering Structures

A Simulation Study on Characterizing Transfer Functions of Railway Tracks Using Train-Borne Laser Doppler Vibrometer

Yuanchen Zeng(✉), Alfredo Núñez, and Zili Li

Delft University of Technology, Delft 2628 CN, The Netherlands
Y.Zeng-2@tudelft.nl

Abstract. Due to train load and aging, the dynamic properties of railway tracks degrade over time and deviate over space, which should be monitored to facilitate track maintenance decisions. A train-borne laser Doppler vibrometer (LDV) can directly measure track vibrations in response to the moving train load, which can be potentially applied to large-scale rail infrastructure monitoring. This paper characterizes track structures as a distributed system by estimating transfer functions between the wheel-rail force and the response of each sleeper measured by a train-borne LDV. A challenge with this technique is that a train-borne LDV measures only a fragment of the response for each sleeper while the train load is moving. To investigate the feasibility of this technique and the influence of key factors, we perform numerical simulations using a vehicle-track model and analyze the estimation performance through comparison with simulated impact hammer tests. We find that the transfer function estimated under a moving excitation is close to but noisier than that estimated under an impact load. Partial measurement affects the estimation performance significantly, and a wider sleeper provides a better estimate and a higher frequency resolution. Train speed is a crucial factor for a train-borne LDV system. As the vehicle speed increases, the estimation performance gets better at high frequencies but worse at low frequencies.

Keywords: Transfer Function Estimation · Railway Tracks · Vibration Measurement · Moving Load · Laser Doppler Vibrometer

1 Introduction

The dynamic properties of railway tracks affect the interaction between trains and tracks and the safety of operation. Due to train load and aging, these properties degrade over time and deviate over space. Monitoring the track dynamic properties can facilitate the decision-making of track maintenance. Transfer functions are an effective representation of such properties in the frequency domain [1–3].

For models of railway tracks, transfer functions can be calculated analytically or numerically, while for railway tracks in real life, transfer functions are usually measured through impact hammer tests [4–6]. In such a test, the excitation is usually generated manually and measured by the hammer, and the track response is usually measured by

M. P. Limongelli et al. (Eds.): EVACES 2023, LNCE 432, pp. 183–192, 2023.
https://doi.org/10.1007/978-3-031-39109-5_19

accelerometers. It has the advantages of low noise or interference, high repeatability, and high coherence. However, it requires human workload, long experiment time, and temporary operation shutdowns [6], so it is mostly applied only at hot spots.

Alternatively, track dynamic properties can be identified from track vibrations under operational conditions [7]. Laser Doppler vibrometer (LDV) is a laser-based sensing instrument that measures the vibration velocity of a target based on the Doppler frequency shift. It has the advantage of non-contact sensing and has been applied to the modal identification and damage detection of many engineering structures [8, 9], while in most applications, an LDV stands statically and measures at discrete points or along a closed path [10]. A train-borne LDV is a novel setup that targets the laser spot on tracks and measures the track vibration in response to the moving train. It has the potential to be used for railway monitoring. In a simulation study [11], train-borne LDVs are used to identify the mode shapes of a bridge. In an experimental study [12], a train-borne LDV is used to identify the rail bending modes.

A train-borne LDV measures the response of railway tracks under the dynamic train load. When wheel-rail contact forces are measured or identified, the transfer function of railway tracks can be estimated. For example, a railway track can be characterized as a distributed system where a transfer function can be calculated for each sleeper using the wheel-rail force and the sleeper response. However, a challenge associated with this technique is that a train-borne LDV measures only a fragment of the response for each sleeper when the train load is moving. To the best of our knowledge, no research has been published on such applications.

In this paper, we conduct a simulation study on the feasibility of transfer function estimation using a train-borne LDV and the influence of its key factors. It should be noted that, in this paper, we assume that wheel-rail forces are directly available. However, in practice, the accurate measurement or identification of wheel-rail forces remains a challenging topic [13, 14].

The remainder of this paper is organized as follows. In Sect. 2, the simulation model and the transfer function estimation method are introduced. In Sect. 3, the influence of several key factors is studied, including the moving excitation and partial measurement. In Sect. 4, some conclusions are summarized.

2 Modeling and Simulation

2.1 A Vehicle-Track Model

We use a vertical vehicle-track model to simulate sleeper vibration measurement using a train-borne LDV, as shown in Fig. 1. The vehicle is represented by a quarter car with two rigid bodies as follows,

$$m_1\ddot{z}_1(t) + k_s[z_1(t) - z_2(t)] + c_s[\dot{z}_1(t) - \dot{z}_2(t)] = 0 \tag{1}$$

$$m_2\ddot{z}_2(t) - k_s[z_1(t) - z_2(t)] - c_s[\dot{z}_1(t) - \dot{z}_2(t)] + f_c(t) = 0 \tag{2}$$

where m_1 and m_2 are the two masses, respectively, k_s and c_s are the suspension stiffness and damping, respectively, z_1 and z_2 are the vertical displacements of the two bodies, respectively, and f_c is the wheel-rail contact force.

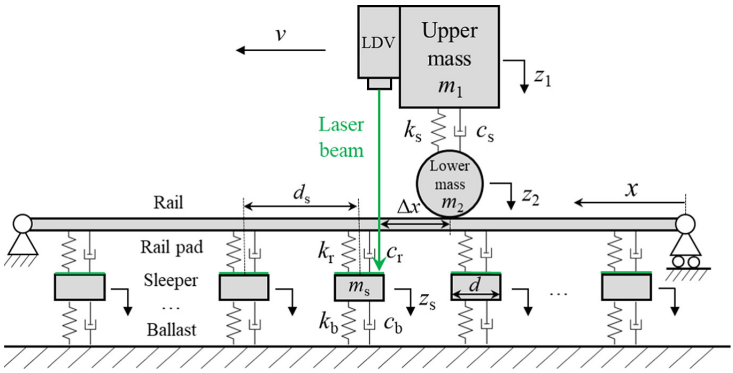

Fig. 1. A vehicle-track model.

In this model, sleepers are also characterized by rigid bodies, and the equation of motion of the i-th sleeper ($i = 1,.., n_s$) is:

$$m_s\ddot{z}_{si}(t) - k_r[z_r(x_{si}, t) - z_{si}(t)] - c_r[\dot{z}_r(x_{si}, t) - \dot{z}_{si}(t)] + k_b z_{si}(t) + c_b\dot{z}_{si}(t) = 0 \quad (3)$$

where m_s is the sleeper mass, z_{si} is the displacement of the i-th sleeper, k_r and c_r are the rail pad stiffness and damping, respectively, k_b and c_b are the ballast stiffness and damping, respectively, x_{si} is the position of the i-th sleeper, i.e., $x_{si} = (i–1/2)d_s$ with d_s the sleeper spacing, and $z_r(x_{si}, t)$ is the displacement of the rail at position x_{si}.

The rail is modeled as a simply-supported Euler-Bernoulli beam of length $l = n_s \times d_s$. Considering the discrete support of the sleepers, the displacement of the beam at position x and time t is characterized as follows [15],

$$\begin{aligned} EI\frac{\partial^4 z_r(x,t)}{\partial x^4} + m_r\frac{\partial^2 z_r(x,t)}{\partial t^2} &= f_c(t)\delta(x - x_c(t)) - \\ \sum_{i=1}^{n_s} k_r[z_r(x_{si}, t) - z_{si}(t)]\delta(x - x_{si}) &- \sum_{i=1}^{n_s} c_r[\dot{z}_r(x_{si}, t) - \dot{z}_{si}(t)]\delta(x - x_{si}) \end{aligned} \quad (4)$$

where E is the elastic modulus of the rail, I is the second area moment of the rail, m_r is the mass of the rail per unit length, $\delta(\cdot)$ is the Dirac function, x_c is the wheel position, i.e., $x_c(t) = x_0 + vt$ with v the vehicle speed and x_0 the initial position.

According to the Ritz method, the k-th modal coordinate is denoted as $q_k(t)$, and the k-th modal function is defined as follows [15].

$$Z_k(x) = \sqrt{\frac{2}{m_r l}}\sin\frac{k\pi x}{l} \quad (5)$$

The displacement of the rail is expressed as follows,

$$z_r(x, t) = \sum_{h=1}^{n_m} Z_h(x)q_h(t) \quad (6)$$

where n_m is the truncated order of modes. Then, Eq. (4) can be converted into the following second-order ordinary differential equations.

$$\begin{aligned}&\ddot{q}_k(t)+\sum_{i=1}^{n_s}c_r Z_k(x_{si})\sum_{h=1}^{n_m}Z_h(x_{si})\dot{q}_h(t)+\frac{EI}{m_r}\left(\frac{k\pi}{l}\right)^4 q_k(t)\\&+\sum_{i=1}^{n_s}k_r Z_k(x_{si})\sum_{h=1}^{n_m}Z_h(x_{si})q_h(t)-\sum_{i=1}^{n_s}k_r z_{si}(t)Z_k(x_{si})\\&-\sum_{i=1}^{n_s}c_r\dot{z}_{si}(t)Z_k(x_{si})=f_c(t)Z_k(x_c(t))\;k=1,\ldots,n_m\end{aligned}\tag{7}$$

The contact force is calculated based on Hertz theory as follows [15],

$$f_c(t)=\begin{cases}\left(\frac{1}{G}[z_2(t)-z_r(x_c,t)-z_e(x_c)]\right)^{3/2} & z_2(t)-z_r(x_c,t)-z_e(x_c)>0\\0 & z_2(t)-z_r(x_c,t)-z_e(x_c)<0\end{cases}\tag{8}$$

where z_e is the rail roughness, G is a contact coefficient for a conical wheel, i.e., $G = 4.57{r_w}^{-0.149}\times 10^{-8}$ m/N$^{2/3}$ with r_w the wheel radius. The rail roughness z_e is generated (spatially spaced by Δx_N) by applying a low-pass Butterworth infinite impulse response filter to Gaussian white noise. As shown in Fig. 2, the spectrum of such artificial spatial noise is smoothly monotonic and maximally flat in the passband, which resembles the decay pattern of rail roughness spectra in real life and enables the wheel-rail force to cover a broad frequency range.

To perform numerical simulations of the vehicle-track model, Eqs. (1)~(3) and (7) are solved using the explicit integration algorithm proposed by Zhai [15], while the contact force is updated at each step according to Eq. (8).

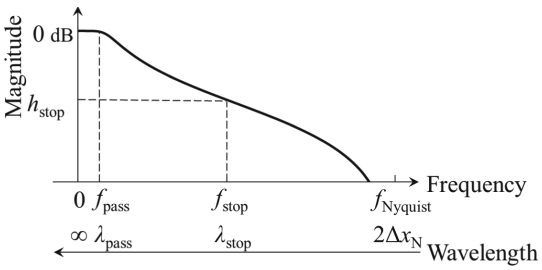

Fig. 2. Spectrum of rail roughness.

The limitations of the above model are discussed as follows.

(1) The vehicle and track are considered linear, so changes in track dynamics due to nonlinearities under a train load cannot be reflected.
(2) The track components are simplified, and the torsion of the rail, the elasticity of the sleepers, and the vibration of the ballast cannot be reflected.

(3) Only a quarter car and half of a track are considered, so the influence of multiple wheels (excitations) cannot be reflected.

Nevertheless, the model is useful and computationally cheap for simulating rigid-body vibrations of sleepers in a multi-layer track structure under a moving vehicle.

2.2 Transfer Function Estimation

A transfer function describes in the frequency domain how a structure at a certain output position responds to an excitation at a certain input position. Railway tracks consist of a continuous rail layer, a discrete sleeper layer, and a continuous ballast layer, and their dynamic properties vary from sleeper to sleeper. Therefore, we define a transfer function for each sleeper as follows, i.e., its frequency response under an excitation on the rail.

$$H_{si}(f) = \frac{Z_{si}(f)}{F_{\mathrm{c}}(f)} \tag{9}$$

where $Z_{si}(f)$ denotes the spectrum of the i-th sleeper displacement $z_{\mathrm{s}i}(t)$ and $F_{\mathrm{c}}(f)$ denotes the spectrum of the wheel-rail contact force $f_{\mathrm{c}}(t)$.

As shown in Fig. 1, an LDV is mounted on the upper mass with the laser spot shifting from the wheel-rail contact point by Δx, referred to as 'wheel-laser shift' in this paper. As the vehicle moves, the laser spot scans along a continuous trajectory, and the vibration of a sleeper can only be measured when the laser spot is on the sleeper. Therefore, assuming that the LDV measurement is free of noise and interference, the LDV signal for measuring the i-th sleeper (of width d) is expressed as follows.

$$y_{\mathrm{s}i}(t) = \dot{z}_{\mathrm{s}i}(t) \text{ when } x_{\mathrm{s}i} - \tfrac{d}{2} < vt + \Delta x < x_{\mathrm{s}i} + \tfrac{d}{2} \tag{10}$$

Meanwhile, the excitation from the wheel moves continuously along the rail. In this paper, we assume that the contact force is measured synchronously and accurately. Therefore, the contact force when measuring the i-th sleeper is expressed below.

$$f_{\mathrm{c}i}(t) = f_{\mathrm{c}}(t) \text{ when } x_{\mathrm{s}i} - \tfrac{d}{2} < vt + \Delta x < x_{\mathrm{s}i} + \tfrac{d}{2} \tag{11}$$

Further, the transfer function of the i-th sleeper can be estimated (the so-called H_1 estimate) using the contact force $f_{\mathrm{c}i}(t)$ and the LDV signal $y_{\mathrm{s}i}(t)$ as follows [16],

$$\hat{H}_{si}(f) = \frac{P_{y_{\mathrm{s}}f_{\mathrm{c}}i}(f)}{2\pi f \cdot P_{f_{\mathrm{c}}f_{\mathrm{c}}i}(f)} \tag{12}$$

where $P_{y_{\mathrm{c}}f_{\mathrm{c}}i}(f)$ is the cross PSD of $f_{\mathrm{c}i}(t)$ and $y_{\mathrm{s}i}(t)$ and $P_{f_{\mathrm{c}}f_{\mathrm{c}}i}(f)$ is the auto PSD of $f_{\mathrm{c}i}(t)$.

2.3 Model Parameters

A typical ballast track structure is selected from [17] as a reference simulation case in this paper, and the parameters are listed in Table 1.

Table 1. Parameters of a reference case.

Symbol	Parameter	Value	Symbol	Parameter	Value
m_1	Upper mass	9000 kg	k_s	Suspension stiffness	100 kN/m
m_2	Lower mass	2700 kg	c_s	Suspension damping	5 kN/(m/s)
r_w	Wheel radius	0.45 m	E	Elastic modulus of rail	210 GPa
m_r	Rail mass per unit length	56 kg/m	n_m	Number of rail modes	25
I	Second area moment of rail	2.231×10^{-5} m^4	n_s	Number of sleepers	25
k_r	Rail pad stiffness	90 MN/m	m_s	Sleeper mass	149 kg
c_r	Rail pad damping	16 kN/(m/s)	d	Sleeper width	0.2 m
k_b	Ballast stiffness	85 MN/m	d_s	Sleeper spacing	0.65 m
c_b	Ballast damping	27.5 kN/(m/s)	Δx	Wheel-laser shift	0 m
λ_{pass}	Passband wavelength of rail roughness	2 m	P_r	Power of Gaussian white noise for rail roughness	−75 dBW
λ_{stop}	Stopband wavelength of rail roughness	5 mm	Δt	Integration step size	1×10^{-5} s

3 Result and Discussion

This section aims to investigate how various factors in the train-borne LDV system affect the performance of transfer function estimation.

3.1 Influence of Moving Excitation

In contrast to hammer tests with fixed impact locations, a train-borne LDV measures the track response when the wheel (excitation) is moving. The influence of such a moving excitation on transfer function estimation is therefore studied.

First, on the established track model (without the vehicle), we apply an impact load in the middle of the rail, which is just on top of the central sleeper, denoted as on-support. This simulates an impact hammer test, and the resulting transfer function is plotted in Fig. 3a. A dominant peak can be observed at 105 Hz, corresponding to the resonance of the sleeper (and the rail) on the ballast. Several peaks can be observed at higher frequencies, corresponding to the resonance and bending of the rail.

Then, we apply a constant moving load superposed with Gaussian white noise along the rail at different speeds. A transfer function is estimated using the applied load and the sleeper vibration when the load is within one sleeper spacing d_s from the central

sleeper. Figure 3a shows that although the transfer functions estimated under the moving load are noisier, they are very close to the one under the impact load.

Further, based on the vehicle-track model, we estimate the transfer function of the central sleeper using the contact force and the sleeper vibration when the wheel is within one sleeper spacing d_s from the sleeper. Figure 3b demonstrates that the transfer function can be well estimated when the vehicle is moving at various speeds.

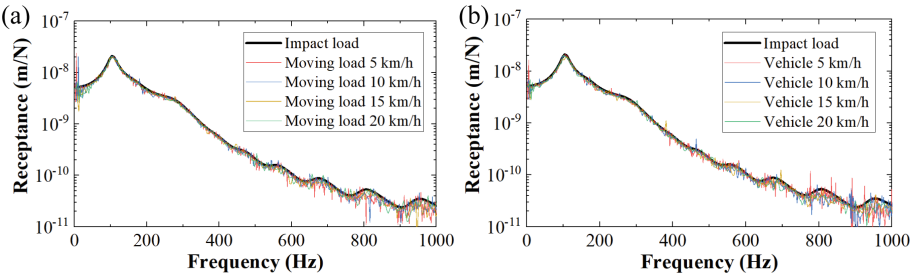

Fig. 3. Influence of moving excitation. (a) Comparison between an impact load and a moving load. (b) Comparison between an impact load and a moving vehicle.

3.2 Influence of Partial Measurement

In Sect. 3.1, the sleeper vibration when the wheel is within one sleeper spacing d_s is used for transfer function estimation. However, for a train-borne LDV, the vibration of a sleeper can only be measured partially, according to Eq. (10), and the signal length of each sleeper depends on the vehicle speed v and the sleeper width d. Therefore, we estimate the transfer function of the central sleeper for different speeds and sleeper widths according to Eqs. (10)~(12), as shown in Fig. 4.

By comparing Fig. 4 with Fig. 3b, we can see that the estimation performance degrades significantly due to the partial measurement, and deviations can be observed near the resonance peak and at high frequencies. The measurements on the wider sleeper provide better estimates and higher frequency resolution than those on the narrow sleeper as a result of longer signal lengths.

For a defined sleeper width, the measurements at low speeds provide good estimates of the resonance peak but quite noisy spectra at high frequencies. Conversely, the measurements at high speeds provide good estimates at high frequencies, but the resonance peak is not well characterized. Two main reasons contribute to this phenomenon: first, for defined track geometry, the frequency of the wheel-rail contact force increases as the speed increases, which excites the high-frequency response of the sleeper more effectively; second, the signal length becomes shorter, and the frequency resolution of the spectrum becomes lower as the speed increases, which makes it more difficult to capture the low-frequency response. The result highlights the significant influence of train speed on the transfer function estimation using a train-borne LDV.

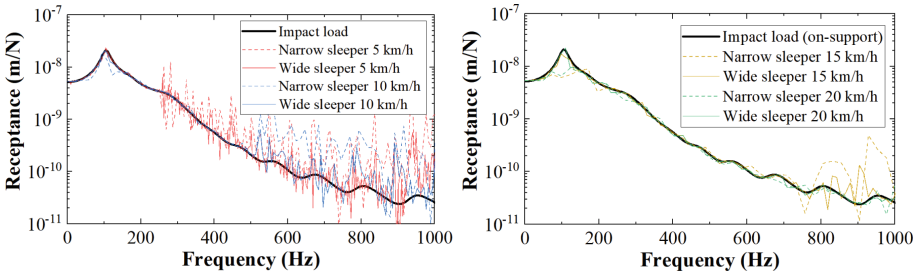

Fig. 4. Influence of partial measurement. 'Wide sleeper' represents a sleeper that is twice as wide as a 'Narrow sleeper' (the reference case).

3.3 Influence of Wheel-Laser Shift

In Sect. 3.2, we assume that the wheel-laser shift Δx is zero, i.e., the LDV measures the track vibration directly below the wheel. Varying the wheel-laser shift Δx affects the excitation position of the sleeper response, which further affects the behavior of the transfer function. Figure 5 shows the transfer functions simulated under impact loads at two different locations, in which $\Delta x = d_s/2$ represents exciting the rail at half the sleeper spacing $d_s/2$ from the central sleeper (known as middle-span) and $\Delta x = d_s$ represents exciting the rail on top of an adjacent sleeper. Then, the estimated transfer functions from train-borne measurements with different Δx are also plotted. It can be seen that the results are similar to those shown in Fig. 4, indicating that the influence of different excitation positions is not significant.

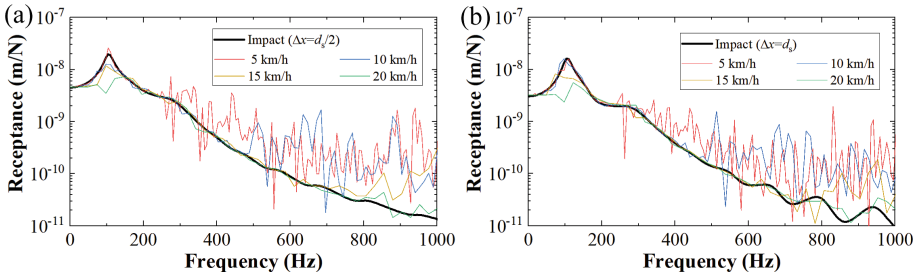

Fig. 5. Influence of wheel-laser shift. (a) $\Delta x = d_s/2$. (b) $\Delta x = d_s$.

3.4 Performance on a New Case

The above simulations are performed based on the reference parameters in Table 1. To further test the performance of transfer function estimation, some parameters are changed to Table 2 based on the parameters in [17]. The key property of this track structure is that the rail pad stiffness k_r is significantly higher than the reference case. As a consequence, the transfer function plotted in Fig. 6 has higher magnitudes at high frequencies, and the resonance frequency is slightly lower. It shows that the transfer function can be estimated with a performance similar to the one shown above.

Table 2. Parameters of a new case.

Symbol	Parameter	Value	Symbol	Parameter	Value
k_r	Rail pad stiffness	1300 MN/m	m_r	Rail mass per unit length	54.77 kg/m
c_r	Rail pad damping	67.5 kN/(m/s)	I	Second area moment of rail	2.337×10^{-5} m^4
k_b	Ballast stiffness	45 MN/m	m_s	Sleeper mass	138.7 kg
c_b	Ballast damping	32 kN/(m/s)	d_s	Sleeper spacing	0.6 m

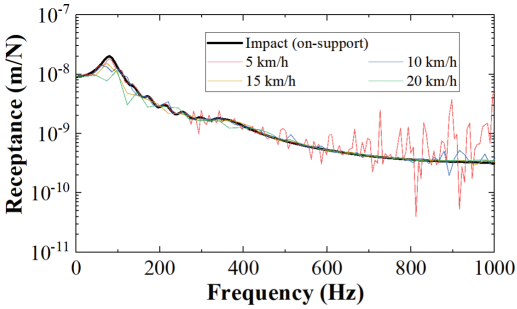

Fig. 6. Transfer function estimation for the new case.

4 Conclusion

This paper investigates the feasibility of transfer function estimation using a train-borne LDV and the influence of several key factors. The main conclusions are drawn below.

(1) The transfer function estimated under the moving excitation is close to but noisier than that estimated under an impact load.
(2) Partial measurement affects the estimation performance significantly. A wider sleeper provides a better estimate and a higher frequency resolution.
(3) As the vehicle speed increases, the estimation performance gets better at high frequencies but worse at low frequencies. This is related to the variation of the contact force frequency and frequency resolution with speed.
(4) Changing the wheel-laser shift and the track stiffness does not affect the estimation performance significantly.

For future research, we will investigate the noise characteristics in a train-borne LDV system based on this preliminary work. Meanwhile, experiments will be performed to further demonstrate this technique.

Acknowledgment. This research was partly supported by ProRail and Europe's Rail Flagship Project IAM4RAIL - Holistic and Integrated Asset Management for Europe's RAIL System [grant agreement 101101966].

References

1. Grassie, S.L., Gregory, R.W., Harrison, D., Johnson, K.L.: The dynamic response of railway track to high frequency vertical excitation. J. Mech. Eng. Sci. **24**(2), 77–90 (1982)
2. Agostinacchio, M., Ciampa, D., Diomedi, M., Olita, S.: Parametrical analysis of the railways dynamic response at high speed moving loads. J. Mod. Transp. **21**(3), 169–181 (2013). https://doi.org/10.1007/s40534-013-0022-y
3. Shen, C., Deng, X., Wei, Z., Dollevoet, R., Zoeteman, A., Li, Z.: Comparisons between beam and continuum models for modelling wheel-rail impact at a singular rail surface defect. Int. J. Mech. Sci. **198**, 106400 (2021)
4. Oregui, M., Li, Z., Dollevoet, R.: Identification of characteristic frequencies of damaged railway tracks using field hammer test measurements. Mech. Syst. Signal Process. **54**, 224–242 (2015)
5. Lam, H.F., Wong, M.T., Yang, Y.B.: A feasibility study on railway ballast damage detection utilizing measured vibration of in situ concrete sleeper. Eng. Struct. **45**, 284–298 (2012)
6. Zeng, Y., Shen, C., Núñez, A., Dollevoet, R., Zhang, W., Li, Z.: An interpretable method for operational modal analysis in time-frequency representation and its applications to railway sleepers. Struct. Control Health Monitor. **2023**, 1–26 (2023). https://doi.org/10.1155/2023/6420772
7. Wang, P., Wang, L., Chen, R., Xu, J., Xu, J., Gao, M.: Overview and outlook on railway track stiffness measurement. J. Mod. Transp. **24**(2), 89–102 (2016). https://doi.org/10.1007/s40534-016-0104-8
8. Lutzmann, P., Göhler, B., Van Putten, F., Hill, C.A.: Laser vibration sensing: overview and applications. Elect. Opt. Rem. Sens. Photon. Technol. Appl. V **8186**, 11–26 (2011)
9. Rothberg, S.J., et al.: An international review of laser Doppler vibrometry: making light work of vibration measurement. Opt. Lasers Eng. **99**, 11–22 (2017)
10. Zeng, Y., Núñez, A., Li, Z.: Speckle noise reduction for structural vibration measurement with laser Doppler vibrometer on moving platform. Mech. Syst. Signal Process. **178**, 109196 (2022)
11. Obien, E.J., Malekjafarian, A.: A mode shape-based damage detection approach using laser measurement from a vehicle crossing a simply supported bridge: a bridge damage detection approach using a passing vehicle. Struct. Control Health Monitor. **23**(10), 1273–1286 (2016). https://doi.org/10.1002/stc.1841
12. Kaynardag, K., Battaglia, G., Ebrahimkhanlou, A., Pirrotta, A., Salamone, S.: Identification of bending modes of vibration in rails by a laser Doppler vibrometer on a moving platform. Exp. Tech. **45**(1), 13–24 (2021)
13. Wei, L., Zeng, J., Wu, P., Gao, H.: Indirect method for wheel-rail force measurement and derailment evaluation. Veh. Syst. Dyn. **52**(12), 1622–1641 (2014)
14. Xia, F., Cole, C., Wolfs, P.: Grey box-based inverse wagon model to predict wheel–rail contact forces from measured wagon body responses. Veh. Syst. Dyn. **46**(S1), 469–479 (2008)
15. Zhai, W.: Vehicle–track coupled dynamics models. Springer, Singapore (2020)
16. Vold, H., Crowley, J., Thomas Rocklin, G.: New ways of estimating frequency response functions. Sound Vibr. **18**, 34–38 (1984)
17. Shen, C., Dollevoet, R., Li, Z.: Fast and robust identification of railway track stiffness from simple field measurement. Mech. Syst. Signal Process. **152**, 107431 (2021)